Journal of Alloys and Compounds 509 (2011) 5796–5803

Contents lists available at ScienceDirect

Journal of Alloys and Compounds

journal homepage: www.elsevier.com/locate/jallcom

Studies on $La_{0.67}Ca_{0.33}MnO_3$–$SrTiO_3$ composites using two-phase model

Sunita Keshri*, Leena Joshi, Shailendra Singh Rajput

Department of Applied Physics, Birla Institute of Technology, Mesra, Ranchi – 835215, Jharkhand, India

ARTICLE INFO

Article history:
Received 12 November 2010
Received in revised form 20 February 2011
Accepted 22 February 2011
Available online 2 March 2011

Keywords:
CMR-based composites
Grain size
Percolation threshold
Two-phase model

ABSTRACT

In this study we report the structural, electrical and magnetic properties of $(1-x)La_{0.67}Ca_{0.33}MnO_3$ (LCMO)–$(x)SrTiO_3$(STO) composites. For this series we have observed a minute change in ferromagnetic (FM)–paramagnetic (PM) transition temperature with STO addition in LCMO matrix; however a reasonable change is observed in metal–insulator transition temperature, along with the occurrence of percolation threshold for $x = 0.30$ sample. Overall pattern for temperature dependence of resistivity for this series has been best-fitted using the formula $1/\rho = (1-f)/\rho_{PM} + (f/\rho_{FM})$, where ρ_{PM} and ρ_{FM} are the resistivities of the PM and FM contents in the sample and f is the volume fraction of FM phase in the sample. Investigations on magnetoresistance (MR) using magnetic field up to 3 T show enhancement of extrinsic MR in the composite samples which can be viewed in the light of spin polarized tunneling.

1. Introduction

Perovskite manganites with chemical formula $R_xA_{1-x}MnO_3$, where R = La, Nd, Pr, etc. trivalent rare-earth ions and A = Sr, Ca, etc. divalent alkaline-earth ions, have attracted considerable research interest in recent years because of the observation of a huge magnetoresistance (MR) in them, called the colossal magnetoresistance (CMR) effect. These materials have unusually strong coupling among their lattices, spins, and charge degrees of freedom [1,2]. These properties find applications in magnetic sensors, magnetic switching of recording devices, magnetic refrigeration, etc. [3,4]. The intrinsic CMR, caused by the double exchange (DE) mechanism proposed by Zener in 1951 [5], is useful to explain CMR phenomena mostly observed near T_C. However the extrinsic CMR, which is absent in a single crystal, is related to natural and artificial grain boundaries (GBs). Spin polarized tunneling or spin dependent scattering of the charge carriers at the GBs seems to be responsible for this kind of CMR effects [2]. This extrinsic effect may enhance MR in a wide temperature range and can be more useful to satisfy practical applications.

For a better understanding of CMR a large number of studies have been carried out in single crystals [6], thin films [7,8], polycrystalline CMR materials [9,10] and CMR-based composites [11–18]. Many groups have attempted to synthesize CMR–insulator composites, such as $La_{0.67}Ca_{0.33}MnO_3$ (LCMO)–MgO [11], LCMO–$BaTiO_3$ (BTO) [12,13], LCMO–Al_2O_3 [14,15], $La_{0.67}Sr_{0.33}MnO_3$–La_2O_3–$La(OH)_3$ [16], $La_{0.67}Sr_{0.33}MnO_3$–polyaniline [17] and LCMO–$SrTiO_3$ (STO) [18], etc. Incorporation of insulating materials as a second phase is believed to be advantageous to enhance extrinsic CMR behaviour as they make the GBs insulating, thus creating a barrier in the way of the charge carriers followed by an enhancement of tunneling probability. The LCMO has been selected as the matrix material by many researchers, because it is one of the well-studied manganites among the large number of pure CMR materials studied so far. In our previous papers, we have reported on the electrical and magnetic properties of LCMO–BTO [12] and LCMO–STO [18] composites. Both these series show a peaky intrinsic MR behaviour at T_C followed by a wide extrinsic MR behaviour below this temperature. Our LCMO–BTO composites have shown extrinsic MR up to 60% (at 20 K) in presence of 3 T magnetic field. But our previous LCMO–STO composites show only up to 35% (at 5 K) for the same magnetic field, although STO is a good insulator and supposed to enhance the electron tunneling probability at the GBs. So our main motivation behind the present investigation is to achieve large MR of LCMO–STO composites for a wide temperature range; we have tried to achieve this by reducing the grain size of LCMO matrix. It is generally expected that a high value of the surface-to-volume ratio with sharper GBs can enhance the MR. Hence studies on such samples with high density GBs seem to be informative. In the present paper, we have studied the structural, electrical and magnetic properties of LCMO–STO series, prepared using LCMO of smaller grain size (100–170 nm as compared to 5–7 μm for previous case) and STO of 25–70 nm grain size (similar to previous one).

The most remarkable feature observed in composite samples is decrease in T_{MI} with the increase of the grain boundary effect whereas there is no significant change in T_C [12,14]. Along with the decrease in T_{MI}, the resistivity curves become broader. Phenomenologically, such transport behaviour can be explained by considering

* Corresponding author. Fax: +91 651 2275401.
E-mail addresses: sskeshri@rediffmail.com, s_keshri@bitmesra.ac.in (S. Keshri).

0925-8388/$ – see front matter © 2011 Elsevier B.V. All rights reserved.
doi:10.1016/j.jallcom.2011.02.122

a two-phase model in which two kinds of conduction channels are connected in parallel to each other. Jaime et al. [19] have used an effective medium approach to compute the total resistivity of the two-component system for LCMO thin films. Their work explores the possibility that a field- and temperature-dependent concentration of metallic regions may occur within a semiconductive, polaronic background having an activated electrical conductivity. This model was further modified by Rubinstein [20] by incorporating the concept of $f(T)$ which defines the fraction of the carriers that are in the metallic state, required as a reasonable function to fit the two halves of the resistivity curve together. Several researchers have considered similar two-phase model for explaining transport behaviours of different CMR based composites, e.g. LCMO–Al_2O_3 [14,15], LCMO–$BaTiO_3$ [13] and LCMO–LCSMO [21], etc. However, working formulae used by them are not exactly same. Moreover, we have not come across this type of work on LCMO–STO composites. Hence in this paper, we have tried to make a theoretical investigation on the effect of STO addition on transport behaviour of LCMO using two-phase model. We have found that the fitted curves are in good agreement with our experimental data.

2. Experimental

In the present investigation, the polycrystalline composite series $(1-x)$LCMO–(x)STO, where $x = 0.0$, 0.10, 0.20, 0.30 and 0.40, were prepared in two steps. Firstly single phase LCMO was prepared from high-purity La_2O_3 (99.99), $CaCO_3$ (99.99%), and $Mn(CH_3COO)_2$ (99.99%) by pyrophoric reaction process [22]. The advantages of this technique are that it results small particle size, good particle size distributions, good compositional control and low sintering temperature. The powder was calcinated at 800 °C and 950 °C, respectively, for 12 h to form a perovskite phase. It was then mixed with fine powder of STO (99.99%) in required ratio and pressed into pellets. The pellets were finally sintered at 900 °C in air for 2 h, and then slowly furnace cooled to room temperature. Crystallographic structure of the specimen was examined at room temperature by a Philips diffractometer using Cu Kα radiation for the range $20^\circ \le 2\theta \le 80^\circ$ with a step size of 0.02. The infrared (IR) transmission spectra were studied at room temperature by standard KBr pellet technique using a Perkin Elmer Fourier transform infrared (FTIR) spectrometer (Spectrum 1000). The surface morphology of the samples was studied using JEOL scanning electron microscope (SEM); equipped with Oxford INCA Energy dispersive X-ray (EDX) Spectrometer. The transmission electron microscope (TEM) observation was performed with Philips (CM200) TEM. Sample for TEM study was prepared by dispersing the powder sample in isopropanol and then depositing the resultant dispersed solution onto holey carbon coated copper grid. The electron diffraction (ED) investigation was also carried out. AC susceptibility measurements were carried out with the variation of temperature down to 100 K where real and imaginary components were resolved using a Stanford lock-in-amplifier. For the resistivity measurement sample was cut into rectangular shape from the prepared pellet and the DC electrical resistivity as a function of temperature down to 5 K was measured using the standard four-probe technique, in absence and presence of magnetic field by means of a 8 T superconducting magnet.

3. Results and discussion

3.1. Structural and microscopic analysis

The phase purity and lattice parameters of the synthesized samples were examined by means of powder X-ray diffraction (XRD) at room temperature. The XRD patterns of $(1-x)$LCMO–(x)STO samples, where $x = 0.0$, 1.0, 0.10, 0.20, 0.30 and 0.40, are shown in Fig. 1. Using 'Checkcell' software we have found that LCMO has an orthorhombic structure with lattice constants $a = 5.469(1)$ Å, $b = 7.706(2)$ Å, and $c = 5.457(1)$ Å having *Pnma* space group whereas pure STO has a cubic structure with lattice constant $a = 3.911(1)$ Å having *Pm3m* space group. It can be seen from this figure that for composite samples, the diffraction peaks caused by the individual phases are distinguishable from each other. With increasing STO content, intensity corresponding to pure LCMO phase decreases and that of STO increases. No additional peak of any other phase is observed, indicating that the chance of interdiffusion between LCMO and STO is negligible. It is thereby believed that the composites of this series consist of two chemically separated (LCMO and STO) phases. The IR transmission spectra of the same series measured at room temperature are shown in Fig. 2. This may be mentioned here that unit cell of LCMO consists of central Mn atom surrounded by six nearest neighbour oxygen ions in octahedral structure, which contains six vibrating modes, but only two of them are IR active. The first peak of this spectrum at ~418 cm^{-1} corresponds to bending mode (ν_b) of bond angle and the strong absorption peak at ~592 cm^{-1} arises from stretching mode (ν_s) of Mn–O bond which involves the internal motion of a change in bond length in MnO_6 octahedral and the band at about 592 cm^{-1} can be caused by the Jahn–Teller effect [12,18,23,24]. In IR spectra of STO two absorption peaks have been observed at ~600 cm^{-1} and

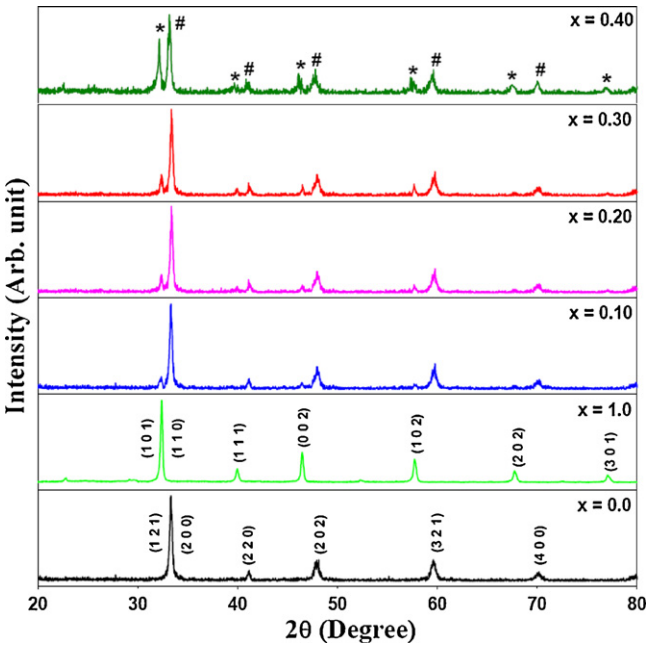

Fig. 1. XRD pattern of $(1-x)$LCMO–(x)STO composite series, where $x = 0.0$, 1.0, 0.10, 0.20, 0.30 and 0.40 [#LCMO and *STO].

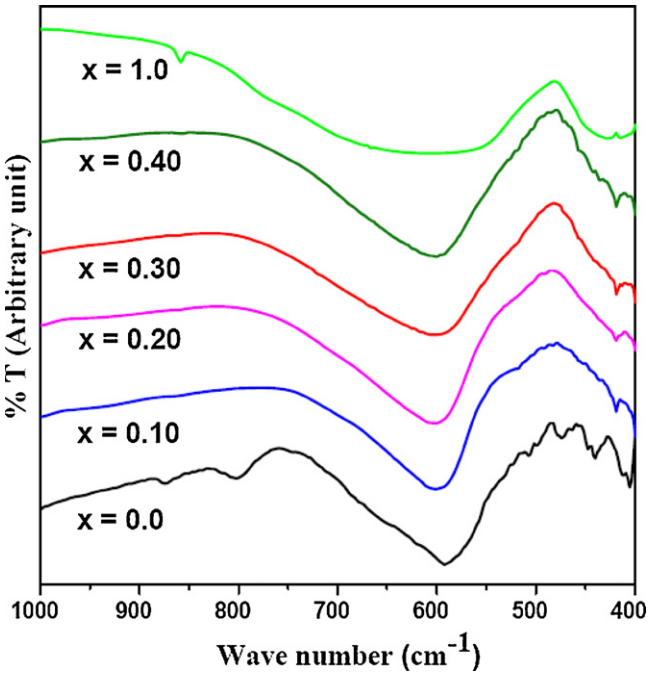

Fig. 2. Infrared spectra of $(1-x)$LCMO–(x)STO samples.

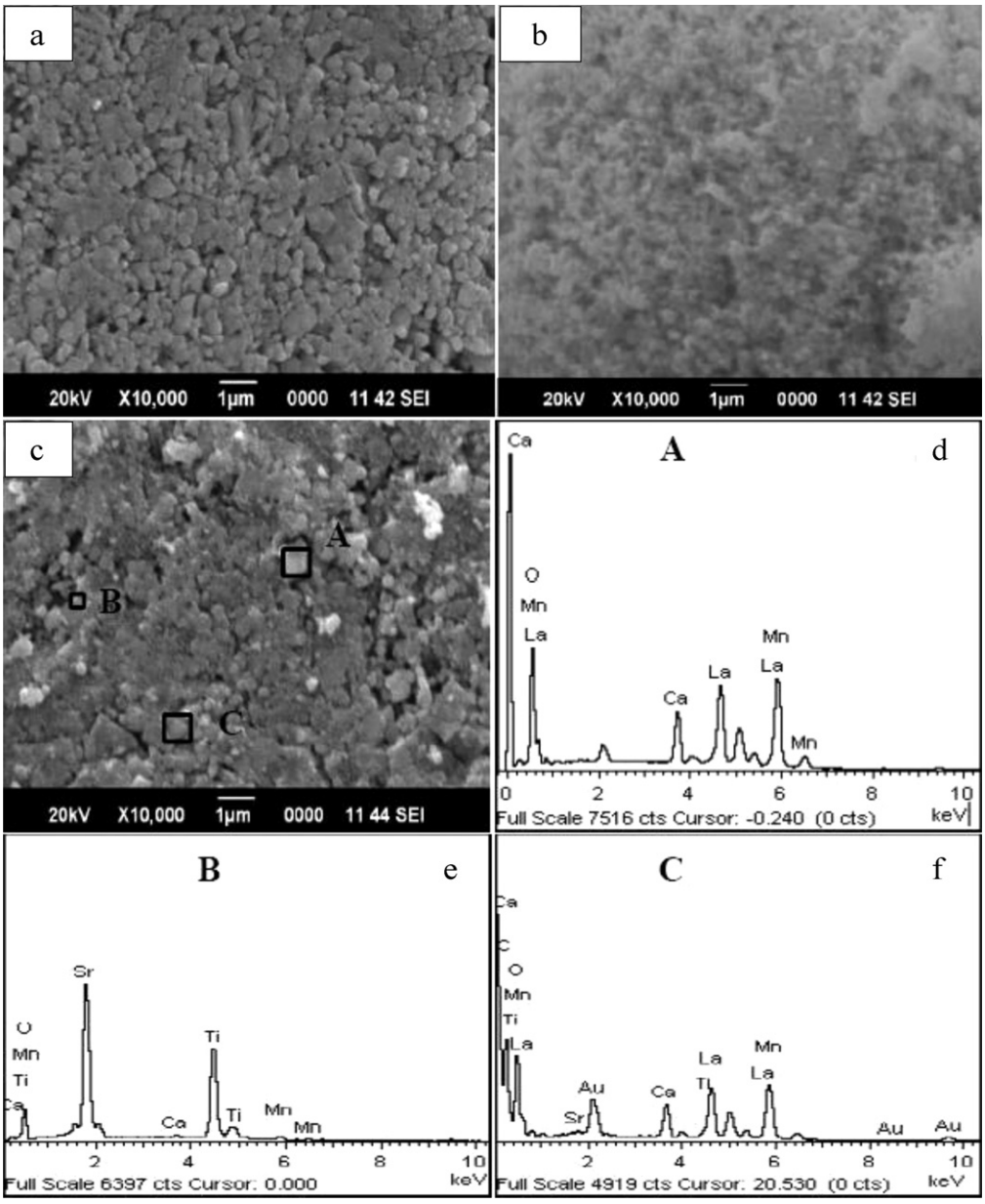

Fig. 3. SEM micrographs of (a) $x = 0$ (LCMO), (b) $x = 0.30$ and (c) $x = 1.0$ (STO powder) samples; (d)–(f) show the EDX results of the regions 'A', 'B' and 'C', respectively.

$\sim$425 cm^{-1} correspond to the Ti–O stretching modes, similar type of result has been found by Zhou et al. [25] also. IR spectra of composite samples contain the absorption peaks of both the phases and no other additional peak. However, it can be observed that the peak width of composite samples at 592 cm^{-1} increases with STO addition. Since absorption peaks at 592 cm^{-1} for LCMO and at 600 cm^{-1} for STO are overlapped for composite samples, chance of minute interdiffusion if any, cannot be understood from FTIR result.

The SEM images of $x = 0$, 0.30 and 1.0 samples are shown in Fig. 3(a)–(c). Both the pure (LCMO and STO) samples have almost homogeneous distribution of spherical grains; grain size of STO is smaller than that of LCMO. From SEM as well as EDX studies we have understood that the STO grains segregate at the grain boundaries and on the surfaces of the LCMO grains. Fig. 3(d)–(f) shows EDX spectrum of three selected positions of $x = 0.30$ sample. As the structural characterization through TEM provides visual demonstration of grain distributions more exactly, we have carried out this study also. The microstructures of $x = 0$, 0.40 and 1.0 samples using TEM are shown in Fig. 4(a)–(c). The micrographs show that the grains of LCMO and STO are nearly spherical in shape. The average grain size of LCMO and STO is found in the range of 100–170 nm and 25–70 nm, respectively. From TEM pattern of $x = 0.40$ sample we find that the two phases, LCMO and STO of different grain sizes are present as individual components in the composite without intermixing. The ED patterns, as shown in Fig. 4(d)–(f), show that diffraction rings are discontinuous and consist of bright spots, indicating that the samples are well crystallized. No dislocations or other extended defects are observed. The ED pattern of $x = 0.40$ composite shows an overlapped appearance constructed as a result of superposition of the diffraction patterns of pure LCMO and STO.

3.2. AC susceptibility

The magnetic behaviour of the grown samples has been analysed by studying temperature variation of real (χ') component of AC susceptibility (Fig. 5). The frequency of AC signal has been kept constant at 131 Hz for entire experiment. The paramagnetic (PM) to ferromagnetic (FM) phase transition temperature which

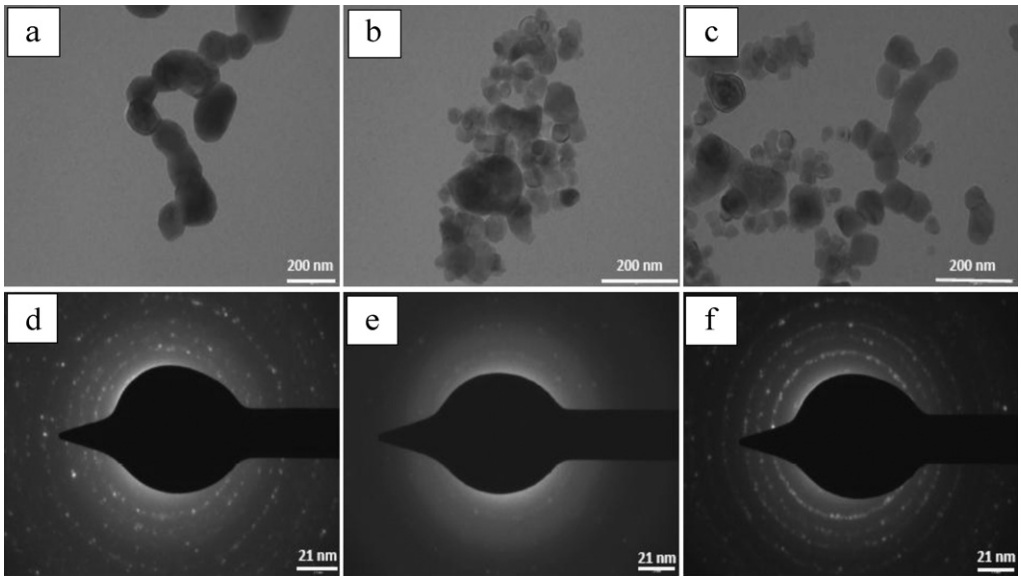

Fig. 4. TEM micrograph of (a) LCMO, (b) $x = 0.40$ sample and (c) STO; (d–f) electron diffraction pattern of the selected area of the corresponding samples.

is known as Curie temperature T_C is determined from minimum point of ($d\chi'/dT$) versus temperature plot. It is observed that on decreasing the temperature below T_C, susceptibility curve shows a small downturn indicating the presence of FM phase with a possible amount of anti-ferromagnetic (AFM) phase [26]. The possible reason of such phenomenon is due to the role of grain boundary and grain surface. The exchange interactions (DE interaction Mn^{3+}–O–Mn^{4+} and AFM super exchange interaction Mn^{3+}–O–Mn^{3+} and Mn^{4+}–O–Mn^{4+}) are weak at grain boundaries compared to those inside the grain [27]. The grain boundary effect becomes more prominent in lower temperature side [12], resulting in a downturn in the χ'–T curve. From Fig. 5 it is evident that a sharp PM–FM transition occurs for LCMO at $T_C = 283$ K. For composite samples with addition of STO, the transition width increases with a minute decrease in T_C, as observed for our LCMO–BTO composites [12] also. From these results we can argue that the magnetic coupling interaction within LCMO grains has not been significantly compressed because of STO addition. The inconsistency of T_C between the pure and composite samples may be due to the different oxygen content in these samples. With the increase in non-magnetic STO content, the volume fraction of LCMO dilutes resulting in a decrease in the value of χ'. Moreover, the existence of STO grains probably causes an increase in grain boundary pinning centers of LCMO grains, prohibiting the hopping of e_g electrons between two neighbour ions below T_C [28]. It may act like a pinning centre for the domain rotation giving rise to a decrease in magnetization [29].

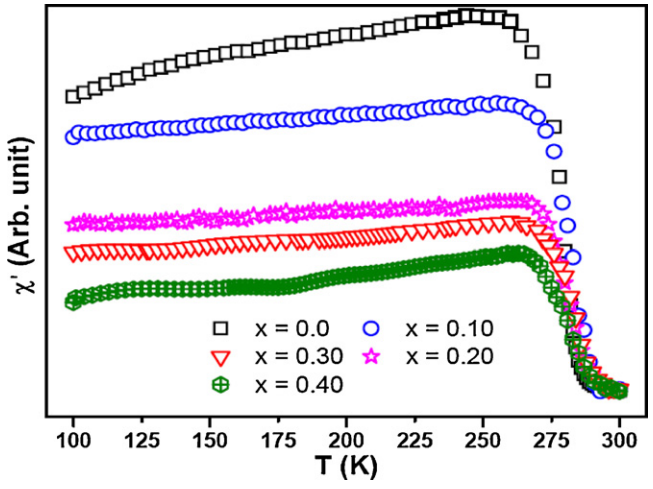

Fig. 5. Real part of AC susceptibility plotted as a function of temperature for $(1-x)$LCMO–(x)STO composite series.

3.3. Resistivity

Temperature dependence of resistivity (ρ) of the pure LCMO and the composite samples is shown in Fig. 6 for the temperature range 5–300 K. Parent sample shows extrinsic metal–insulator (M–I) transition at temperature $T_{MI} = 231$ K with an indistinct peak corresponding to intrinsic M–I transition nearly at $T_C = 283$ K; whereas composite samples show hump type extrinsic transition only. While comparing these results with that for previous series [18], as shown in inset of Fig. 6, we find that the previous parent sample shows only intrinsic M–I transition around T_C whereas its composite samples show double hump corresponding to both types of transitions. In present case the order of resistivity is enhanced by $\sim 10^2$ times compared to that for previous series. These findings can be interpreted as follows. For composite samples with addition of insulating phase there exist two kinds of conduction channels connected parallel: one is the direct contact between CMR grains and the other is through insulating grains [12,18]. Composite samples of present series have more contact area with smaller core, resulting in reduced conductive channels compared to that of previous series. Thus extrinsic behaviour dominates for the first one, which reflects in resistivity behaviour in the form of occurrence of extrinsic peak only with disappearance of intrinsic one.

Fig. 6 shows that with the increase in percentage of STO, T_{MI} shifts towards lower value till $x = 0.30$ and resistivity increases. However for $x = 0.40$ these trends reverse and a percolation threshold is observed for $x = x_m \sim 0.30$. A similar behaviour has also been observed in case of many other CMR based composites [12,18,30]. Suppression of transition temperature to the lower value up to 30% increase in STO suggests towards the suppression of the DE mechanism across the grain boundaries and the average size of LCMO cluster decreases with increase in intergranular effect. However for further increase in STO content (40%), the smaller STO grains start clustering because of which LCMO grains constitute a three-dimensional percolation connection without being surrounded completely by the STO phase and as a result charge carriers find an alternate path showing a decrease in resistivity.

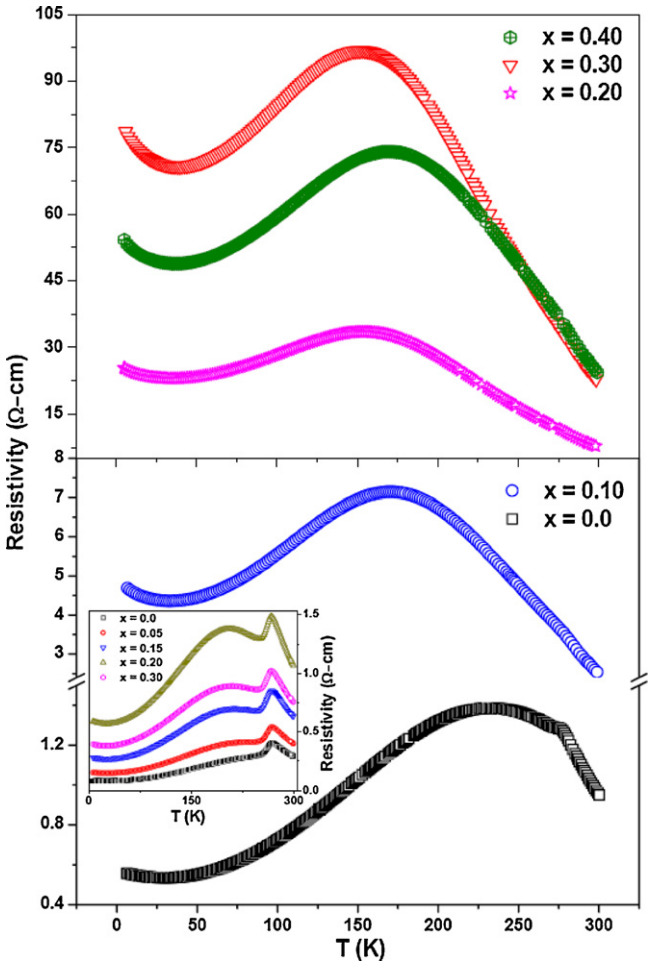

Fig. 6. (a) and (b) Resistivity of the present composite series in the temperature range 5–300 K. Inset shows the resistivity data of our previous LCMO–STO series [16].

Fig. 7(a) shows the normalized resistivity as a function of temperature for the complete series. At sufficiently low temperature (~35 K) a noticeable resistivity minimum is observed for each sample, following an upturn on further decrease in temperature. It is observed that the upturn in the resistivity increases with addition of STO phase till $x = 0.30$ and again decreases for $x = 0.40$. This is another extrinsic effect commonly found in polycrystalline samples [31,32]. We have noticed a steeper low-temperature resistivity upturn for this series compared to that for previous series because of reduction of grain size. When the grain size is small the energy barrier at sufficiently low temperature is quite large, so the charge carriers are inhibited from tunneling from grain to grain giving rise to a steeper rise in resistivity. As the average grain size increases the contribution from Coulomb barriers decreases and charge carriers find enough energy to tunnel through the grains and upturn become less significant. According to a theoretical model proposed by Sheng et al. [33], resistivity for this region can be represented by the equation.

$$\rho(T) = A \exp\left(\sqrt{\frac{\Delta}{T}}\right), \tag{1}$$

with $\Delta \sim E_C$ where E_C is the charging energy. Fig. 7(b) shows the plots of $\rho(T)/\rho(300)$ versus $1/\sqrt{T}$ curve in the lowest temperature regime which exhibits a linear dependence up to ~35 K. The slope of individual fit is proportional to an electrostatic Coulomb energy barrier between the grains. The value of E_C from these fits have been found to be 0.001, 0.236, 1.59, 3.29 and 0.62 K for $x = 0.00$, 0.10, 0.20, 0.30 and 0.40, respectively. It has been observed that E_C increases till $x = 0.30$ sample, which corresponds to percolation threshold. It is because of the fact that with the increase in STO till this sample, average grain size decreases due to the smaller grain size of STO as compared to LCMO. However for $x = 0.40$ sample the smaller STO grains tend to form a cluster like structure; as a results the average grain size increases and thereby E_C decreases compared to that for $x = 0.30$. Our findings are in agreement to that of Phong et al. [14] who have fitted their low temperature resistivity data of nanocrystalline LCMO–Al_2O_3 composite sample using the same model.

The temperature-dependence of the composite series in presence and absence of 3 T magnetic fields is shown in Fig. 8(a)–(e). Previous studies [34,35] show that the resistivity data for such samples in metallic region ($T < T_{MI}$) are governed by electron scattering process and fit well with an equation of the type

$$\rho_{FM} = \rho_0 + \rho_2 T^2, \tag{2}$$

where ρ_0 is the resistivity due to the domains, GBs and other temperature independent scattering mechanism, where the T_2 term is indicative of a combined effect of scattering of electron–electron, electron–phonon and electron–magnon [14]. The $\rho_{FM}(T)$ data fits well with the above equation. On the other hand in insulating regime ($T > T_{MI}$), PM insulating phase is dominated by the hopping motion of self-trapped small polarons [36]. The conventional expression for $\rho(T)$ in this region is as follows:

$$\rho_{PM} = \rho_\alpha T \exp\left(\frac{E_A}{k_B T}\right), \tag{3}$$

where ρ_α is a constant and E_A is the activation energy and k_B is Boltzmann constant. The variation of resistivity in presence of 0 and 3 T magnetic fields have been compared in Fig. 8(a)–(e); with the application of field the indistinct peak corresponding to intrinsic M–I transition of the pristine sample disappears. The addition of STO and the magnetic spin disorder interfaces play the role of energy barriers for the conduction electron and hence lead to an increase in resistivity in the absence of an external magnetic field. When the field is applied, spin disorder is suppressed and within the disordered region Mn spin realign along the direction of field; as a result the tunneling resistivity substantially reduces.

For such a two-phase system, transport properties can be determined by percolation mechanism and resistivities of the entire composite series, with and without magnetic field, can be written as:

$$\frac{1}{\rho} = \frac{(1-f)}{\rho_{PM}} + \frac{f}{\rho_{FM}}, \tag{4}$$

where ρ_{PM} and ρ_{FM} are the resistivities of the PM and FM contents in the sample as given in Eqs. (2) and (3), respectively, and f is the volume fraction of FM phase in the sample. The temperature and field dependence of phase fraction $f(T,H)$ can be given by phenomenological equation

$$f(T,H) = \frac{1}{1 + \exp\{\Delta U(T,H)/k_B T\}}, \tag{5}$$

where ΔU is the energy difference between the metallic and insulating states and may be expressed as:

$$\Delta U \sim -U_0 \left(\frac{1-T}{T_C^{mod}}\right). \tag{6}$$

The ground is the FM state which is of lower energy than insulating state, hence in this expression $-U_0$ is taken as the maximum energy difference for temperature region well below transition temperature. Eq. (5) describes that the value of FM phase fraction f is zero and unity below and above T_{MI}, respectively. The parameter

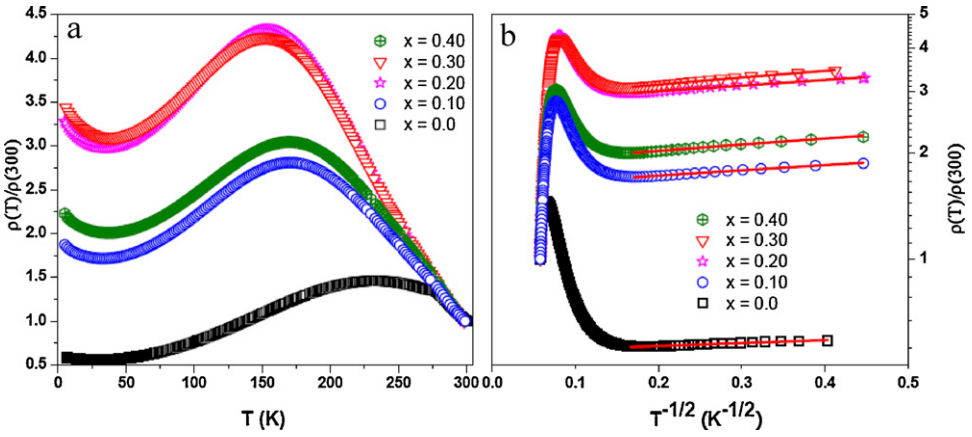

Fig. 7. (a) Normalized reduced resistivity versus temperature for the same series. (b) Plots of $\rho(T)/\rho(300\,\mathrm{K})$ versus $1/\sqrt{T}$, where symbols are the experimental data points and the solid line corresponding to each sample denotes the low temperature resistivity fit to the Eq. (1).

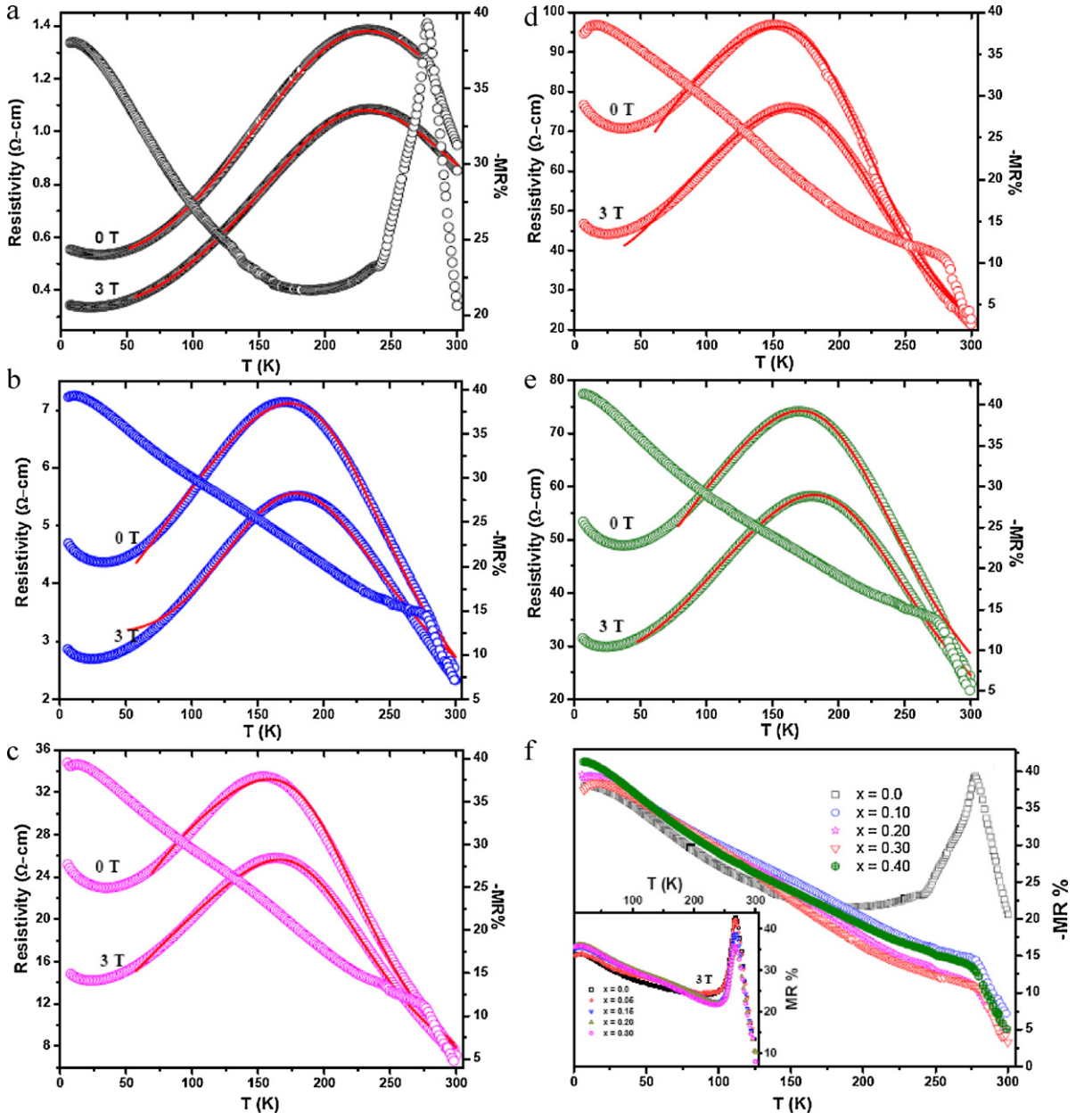

Fig. 8. (a–e) Temperature dependence of resistivity at 0 and 3 T and MR for $(1-x)$LCMO–(x)STO samples. Symbols are the experimental results and solid lines are the graphs fitted by Eq. (4). (f) Temperature variation of MR of all samples at 3 T magnetic field. Inset shows the MR of our previous LCMO–STO series at 3 T [16].

Table 1
T_{MI}, T_C and the parameters obtained corresponding to the best fit by Eq. (4) to the experimental data of $(1-x)$LCMO–(x)STO composite samples, where $x = 0.0$, 0.10, 0.20, 0.30 and 0.40.

Sample	ρ_0 (Ω cm)	$\rho_2 \times 10^{-5}$ (Ω cm K^{-2})	$\rho_a \times 10^{-4}$ (Ω cm)	E_A/k_B (K)	U_A/k_B (K)	T_C^{mod} (K)	T_{MI} (K)	T_C (K)
0 T								
$x = 0.0$	0.53	0.61	0.44	1356	251	232	231	283
$x = 0.10$	3.87	LO	0.66	1430	160	178	170	283
$x = 0.20$	17.53	0.1	1.5	1507	125	154	154	280
$x = 0.30$	49.21	3.35	2.51	1610	91	151	152	280
$x = 0.40$	39.36	0.01	4.1	1570	165	169	170	281
3 T								
$x = 0.0$	0.34	0.70	0.36	1296	247	235	234	–
$x = 0.10$	2.64	1.21	0.65	1410	210	ISO	181	–
$x = 0.20$	13.82	0.18	1.6	1443	189	163	163	–
$x = 0.30$	39.58	2.6	3.2	1574	156	161	162	–
$x = 0.40$	31.57	0.01	0.44	1540	240	181	180	–

T_C^{mod} has been considered as the theoretical value of T_C by some researchers [14,36] earlier. However Li et al. [36], who have used the same model (with temperature dependent volume fraction) for extrinsic transition behaviour ($T_C > T_{MI}$) of LCMO and LCMCO thin films, have obtained T_C^{mod} nearly equal to T_{MI}. Our samples also show extrinsic transition behaviour ($T_C > T_{MI}$) and fittings of our data with Eq. (4) result ($T_C^{mod} \sim T_{MI}$) for each sample; the best-fitted values of all fitting parameters are enlisted in Table 1. From Eqs. (4)–(6) it is evident that near T_C^{mod} the resistivity tends to attain its maximum due to the competition between the contributions of insulating and metallic regions, whereas Eq. (4) illustrates that the resistive behaviour of these samples is strongly dependent upon f. We have found that our data can be fitted well by these equations; the best fit curves using Eq. (4) are shown by solid line in Fig. 8(a)–(e) and experimental data are represented by symbols. However, these equations have not been found adequate to interpret the upturn of resistivity curve at very low temperature region (below 50 K).

From Table 1 it is evident that E_A/k_B and ρ_0 increase with STO content till $x = 0.30 \sim x_m$, after which the trends reverse. Similar sequences have been observed in presence of magnetic field too. This is because; the extrinsic behaviour dominates till the threshold value thereby increasing the parameter ρ_0, which strongly depends on GBs. This also results in increase in activation energy of transport process of carriers. With the application of field, spin fluctuations are suppressed thereby decreasing E_A. The values of E_A/k_B are found to be in the range 1356–1610 and 1296–1574 with and without magnetic field respectively for our samples. It is interesting to see that these values are in agreement with the findings of several authors [14,36]. From Table 1 it is also evident that U_0/k_B decreases with STO content till $x \sim x_m$, and then again increases for $x = 0.40$. Our findings indicate that for our series the energy difference between the metallic and insulating states is lesser.

3.4. Magnetoresistance

The MR is defined as $[\{\rho(H) - \rho(0)\}/\rho(0)] \times 100\,\%$, where $\rho(0)$ and $\rho(H)$ are resistivity values in zero and applied fields respectively. MR as a function of temperature measured in the presence of 3 T magnetic fields is presented for all samples in Fig. 8(f). A sharp peak is observed for the parent LCMO sample corresponding to intrinsic M–I transition nearly at $T_C = 283$ K, whereas from the same temperature MR of composite samples of this series increases almost linearly with the decrease in temperature. These findings indicate that because of incorporation of STO in LCMO, the MR property of the samples becomes completely extrinsic in behaviour. But for our previous LCMO–STO composite series we have found that the intrinsic MR decreases with STO addition while extrinsic MR gets enhanced until a threshold condition is achieved and after this the trend is reversed [18]. The MR values for present series are of larger values compared to the previous series; this enhancement of MR can be attributed to the enhanced and sharper GB effects which also makes the behaviour extrinsic type. This is important to note that for this series we have obtained almost linear temperature dependent extrinsic MR at temperatures below T_C; highest MR achieved for this series is 41% at 5 K as compared to 35% for same temperature for the previous series.

4. Conclusions

In conclusion, we have presented detailed studies of structural, electrical and magnetic behaviours of LCMO–STO composite series. With STO addition, a minute change in T_C with a reasonable change in $T_{MI}(<T_C)$ are observed along with the occurrence of percolation threshold for $x = 0.30$ sample. The resistivity upturn below 35 K can be understood in light of Coulomb blockade model. The overall resistivity data, except for very low temperature region (below 50 K) are found to be fitted well by considering a two-phase model [Eqs. (2)–(5)] in which two kinds of conduction channels are connected to each other, where resistivity in FM metallic region $T < T_{MI}$ is governed by electron scattering process and that in PM insulating phase is dominated by the hopping motion of self-trapped small polarons. To fit the two halves of the resistivity curve together, a function $f(T)$ has been considered which defines the fraction of the carriers that are in the metallic state. From this study it can be understood that the composite samples have sharper GBs compared with those for pure LCMO, resulting a disappearance of intrinsic MR and an enhancement in extrinsic MR as compared to that for pure LCMO. The observed enhanced extrinsic MR in the composite samples has been viewed in the light of spin polarized tunneling. The linear behaviour of temperature dependent MR for a wide temperature range below T_C, as observed for these composites, could be useful for practical applications.

Acknowledgements

S. Keshri gratefully acknowledges Department of Science and Technology (DST), for sanctioning the project. L. Joshi and S.S. Rajput gratefully acknowledge Council of Scientific and Industrial Research and DST for their fellowships, respectively. The authors would like to acknowledge Dr. R. Rawat, UGC-DAE Consortium for Scientific Research, Indore Centre, India, for providing the MR facility. The authors are thankful to the members of Central Instrumentation Facility Lab, Birla Institute of Technology, Mesra for providing SEM and EDX facilities. For the work of XRD and TEM, respectively, the members of Experimental Condensed Matter Physics Division of Saha Institute of Nuclear Physics and Sophisti-

cated Analytical Instrumental Lab of Indian Institute of Technology, Bombay are hereby acknowledged by the authors.

References

[1] A.J. Millis, B.I. Shraiman, R. Muller, Phys. Rev. Lett. 77 (1996) 175–178.
[2] H.Y. Hwang, S.W. Cheong, N.P. Ong, B. Balogg, Phys. Rev. Lett. 77 (1996) 2041–2044.
[3] V.P.S. Awana, R. Tripathi, N. Kumar, H. Kishan, G.L. Bhalla, R. Zeng, L.S. Sharth Chandra, V. Ganesan, H.U. Habermeier, J. Appl. Phys. 107 (2010) 09D723.
[4] D. Rubi, J. Fontcuberta, M. Lacaba, A.M. González, J. Baztán, A. Calleja, Ll. Aragonés, X.G. Capdevila, M. Segarra, Sens. Actuators A 132 (2006) 52–55.
[5] C. Zener, Phys. Rev. 82 (1951) 403–405.
[6] R. von Helmolt, J. Wecker, B. Holzapfel, L. Schultz, K. Samwer, Phys. Rev. Lett. 71 (1993) 2331–2333.
[7] D.R. Sahu, J. Alloys Compd. 503 (2010) 163–169.
[8] K.X. Jin, S.G. Zhao, C.L. Chen, L.F. Du, Y.C. Du, Y.H. Guo, H. Xing, J. Alloys Compd. 470 (2009) 552–556.
[9] R.N. Mahato, K. Sethupathi, V. Sankaranarayanan, R. Nirmala, J. Magn. Magn. Mater. 322 (2010) 2537–2540.
[10] D.H. Manh, P.T. Phong, T.D. Thanh, L.V. Hong, N.X. Phuc, J. Alloys Compd. 499 (2010) 131–134.
[11] H. Yang, Z.E. Cao, X. Shen, T. Xian, W.J. Feng, J.L. Jiang, Y.C. Feng, Z.Q. Wei, J.F. Dai, J. Appl. Phys. 106 (2009) 104317 (1–7).
[12] S. Keshri (Shaw), L. Joshi, S.K. Rout, J. Alloys Compd. 485 (2009) 501–506.
[13] G.M. Ren, S.L. Yuan, G.Q. Yu, J.H. Miao, X. Xiao, H.G. Guan, Y.Q. Wang, S.Y. Yin, J. Phys. D: Appl. Phys. 39 (2006) 4867–4871.
[14] P.T. Phong, N.V. Khiem, N.V. Dai, D.H. Manh, L.V. Hong, N.X. Phuc, Mater. Lett. 63 (2009) 353–356.
[15] L.E. Hueso, J. Rivas, F. Rivadulla, M.A. Lopez-Quintela, J. Appl. Phys. 89 (2001) 1746–1750.
[16] S.P. Liu, G.D. Tang, Z.Z. Li, W.H. Qi, D.H. Ji, Y.F. Li, W. Chen, D.L. Hou, J. Alloys Compd. 509 (2011) 2320–2325.
[17] K. Gupta, P.C. Jana, A.K. Meikap, T.K. Nath, J. Appl. Phys. 107 (2010) 073704 (1–7).
[18] L. Joshi, S.S. Rajput, S. Keshri, Phase Transit. 83 (2010) 482–490.
[19] M. Jaime, P. Lin, S.H. Chun, M.B. Salamon, P. Dorsey, M. Rubinstein, Phys. Rev. B 60 (1999) 1028–1032.
[20] M. Rubinstein, J. Appl. Phys. 87 (2000) 5019–5021.
[21] P.T. Phong, N.V. Dai, D.H. Manhb, T.D. Thanh, N.V. Khiem, L.V. Hong, N.X. Phuc, J. Magn. Magn. Mater. 322 (2010) 2737–2741.
[22] S. Keshri, V. Dayal, Pramana 70 (2008) 697–704.
[23] K.S. Shankar, A.K. Raychaudhuri, J. Mater. Res. 21 (2006) 27–33.
[24] B.M. Nagabhushana, R.P.S. Chakradhar, K.P. Ramesh, C. Shivakumara, G.T. Chandrappa, Mater. Chem. Phys. 102 (2007) 47–52.
[25] N. Zhou, G. Chen, H.J. Zhang, C. Zhou, J. Alloys Compd. 477 (2009) L17–L20.
[26] L. Joshi, V. Dayal, N. Rama, S. Keshri, J. Alloys Compd. 479 (2009) 879–882.
[27] Z.H. Wang, T.H. Ji, Y.Q. Wang, X. Chen, R.W. Li, J.W. Cai, J.R. Sun, B.G. Shen, C.H. Yan, J. Appl. Phys. 87 (2000) 5582–5584.
[28] Y. Wang, Y. Han, C. Zhu, Chin. J. Chem. Phys. 22 (2009) 406–410.
[29] Z.C. Xia, M.T. Hu, F.R. Zeng, G. Liu, B. Dong, L.X. Xiao, L. Liu, S. Liu, C.Q. Tang, S.L. Yuan, Phys. Status Solidi 242 (2005) 1705–1711.
[30] E. Bose, S. Taran, S. Karmakar, B.K. Chaudhuri, S. Pal, C.P. Sun, H.D. Yang, J. Magn. Magn. Mater. 314 (2007) 30–36.
[31] S.K. Mandal, T.K. Nath, V.V. Rao, J. Phys.: Condens. Matter 20 (2008) 385203 (1–12).
[32] P. Dey, T.K. Nath, Phys. Rev. B 73 (2006) 214425 (1–14).
[33] P. Sheng, B. Abeles, Y. Arie, Phys. Rev. Lett. 31 (1973) 47–51.
[34] N. Panwar, D.K. Pandya, S.K. Agarwal, J. Phys. D: Appl. Phys. 40 (2007) 7548–7575.
[35] J.B. Goodenough, J.S. Zhou, Nature 386 (1997) 229–230.
[36] G. Li, H.D. Zhou, S.J. Feng, X.J. Fan, X.G. Li, Z.D. Wang, J. Appl. Phys. 92 (2002) 1406–1410.